

# Dispersion from ground-level sources in a shoreline urban area

Jing Yuan<sup>a</sup>, Akula Venkatram<sup>a,\*</sup>, Vlad Isakov<sup>b</sup>

<sup>a</sup>Department of Mechanical Engineering, University of California, Riverside, CA 92521, USA

<sup>b</sup>NOAA/Atmospheric Sciences Modeling Division,<sup>1</sup> USA

Received 23 May 2005; received in revised form 7 October 2005; accepted 7 October 2005

## Abstract

We present results from a field study conducted in Wilmington, a suburb of Los Angeles, during 8 days of the period 26 August–10 September 2004. The tracer, sulfur hexafluoride, was released at a height of 3 m from a power plant site on the shoreline, and the concentrations of the tracer were sampled on five arcs at 100, 400, 1000, 3000, and 5000 m from the source during 6 h of the day starting at 7 a.m. This resulted in 40-h-long experiments, out of which, 21 had concentration measurements that could be interpreted with models. The meteorological conditions that governed dispersion were measured using sonic anemometers and sodars. The data analysis indicates that even during summer, the stability of the onshore flow is strong enough to keep the height of the convective internal boundary layer below 150 m at distances of 5000 m from the shoreline. However, the turbulence levels in the stable boundary layer are not smaller than those in the surface convective layer suggesting the presence of a shear generated boundary layer, which is advected with the onshore flow.

A simple Gaussian dispersion model was used to interpret the ground-level concentrations measured in the experiment. The model uses expressions for plume spreads that depend on meteorological information at a height of 50 m from the surface. The vertical spread of the plume is limited to the height of the shear generated boundary layer. The height of this boundary layer is proportional to  $\sigma_w/N$ , where  $\sigma_w$  is the standard deviation of the vertical velocity fluctuations, and  $N$  is the Brunt–Vaisala frequency of the stable layer capping the surface-based convective layer. This result is based on indirect evidence: model performance improves significantly when vertical plume spread is limited to this height.

© 2005 Elsevier Ltd. All rights reserved.

**Keywords:** Shoreline dispersion; Shear generated boundary layer; Field experiment; Tracer study; Plume spread; Dispersion model; Data analysis; Wilmington; Urban dispersion; Thermal internal boundary layer

## 1. Introduction

The rapid expansion of industrial and commercial operations near shorelines has created a critical

need for dispersion models that provide reliable assessment of exposures to air toxics released from shoreline sources. These dispersion models need to account for the effects of the thermal internal boundary layer (TIBL), which is the convective boundary layer that develops when stable air over the water flows onto warmer land. The TIBL grows with distance from the shoreline. Research over the past 30 years has resulted in several dispersion models that account for the effects of the TIBL on

\*Corresponding author. Tel.: +1 951 827 2195; fax: +1 951 827 2899.

E-mail address: [venky@engr.ucr.edu](mailto:venky@engr.ucr.edu) (A. Venkatram).

<sup>1</sup>In partnership with the US Environmental Protection Agency, Research Triangle Park, NC 27711, USA.

dispersion (Misra and Onlock, 1982; Luhar and Sawford, 1996). However, most of these models focus on elevated releases and the associated ground-level fumigation when the elevated plume intersects the growing TIBL. Few studies have examined dispersion of near ground-level emissions, which represent most urban air toxics sources near shorelines.

In this paper, we interpret the behavior of plume spreads and concentrations associated with surface releases in a coastal urban area using flow and turbulence variables measured in the urban boundary layer. The observations used in this study were obtained from a field experiment conducted in Wilmington, CA, which is located on the coast, south of Los Angeles. We first provide a description of the experimental design and implementation of the field study.

## 2. Wilmington field study

The major objective of the Wilmington field study, sponsored by California Air Resources Board (CARB) and California Energy Commission

(CEC), was to formulate and evaluate a short-range dispersion model for sources in coastal urban areas. The field experiment was conducted by the University of California, Riverside (UCR) near the Harbor Generating Station of the City of Los Angeles' Department of Water and Power (LADWP), in Wilmington, CA. Wilmington is a community of about 53,000 people located next to the Port of Los Angeles. It is surrounded by numerous small industries, transportation corridors, and port businesses, which are located to the south of residential areas. Fig. 1 shows the map of Wilmington. The residential areas, consisting mostly of one-story buildings of about 4 m high, are located downwind of the release point inside the LADWP site during the dominant southeasterly flows. The building density is relatively low, suggesting flow in which wake interference is small.

### 2.1. Tracer concentration measurements

Tracer studies were conducted on 8 days during the period 26 August–10 September 2004. Each study day involved release of the tracer gas, sulfur

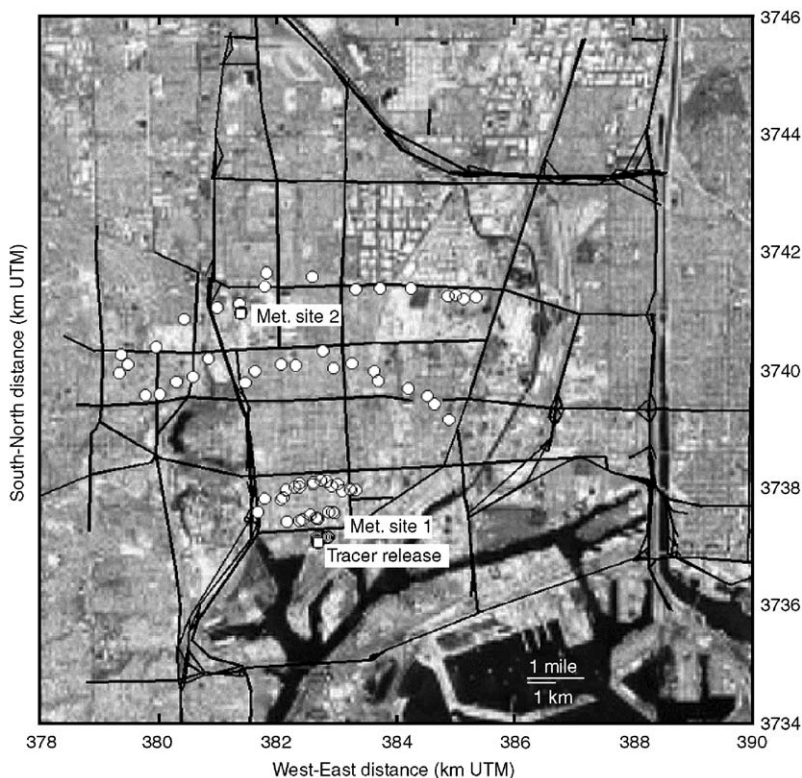


Fig. 1. Map of study area and equipment locations.

hexafluoride ( $\text{SF}_6$ ), over periods lasting from 2 to 6 h. During the first 6 days, pure  $\text{SF}_6$  was metered with a mass flow controller and mixed with  $100 \text{ L min}^{-1}$  of ambient air provided by a vane pump to change the buoyancy of the gas to nearly that of the surrounding air. The diluted  $\text{SF}_6$  was released at a rate of  $4 \text{ g s}^{-1}$  ( $16 \text{ kg h}^{-1}$ ) at the base of a stack of the LADWP generating station, which is located  $\sim 0.8 \text{ km}$  from the ocean, adjacent to the Port of Los Angeles. During the last 2 study days, the diluted  $\text{SF}_6$  was directed into a 3-m tall piece of 1" PVC pipe supported by a tripod in an open area inside the generating station. The  $\text{SF}_6$  exited at the top of the tube had a 2" PVC diffuser cap designed to generate a neutrally buoyant plume. The  $\text{SF}_6$  tracer gas release rate was  $2 \text{ g s}^{-1}$  ( $8 \text{ kg h}^{-1}$ ) for these tests.

The released tracer was sampled along five arcs. Three of the arcs were located at  $\sim 1000$ , 3000, and 5000 m from the release point. The fourth and fifth set of samplers were placed along radial distances ranging between 100 and 400 m from the source. Eighteen samplers were placed at  $6^\circ$  spacing on the 1000 and 3000 m arcs, while eight and 11 samplers were placed  $\sim 5^\circ$  apart on the 100 and 400 m arcs, respectively. There were 17 samplers on the 5000 m arc, with two additional samplers collocated at the two sites for quality control purposes. The locations of these samplers are also shown in Fig. 1. Measurements on a mobile monitoring van using a real-time continuous monitor were used to supplement those from the stationary integrated samplers.

Gas samplers, designed and constructed at UCR, were used to collect integrated samples over consecutive 1-h time periods. Each sampler included a timer that controlled six air-sampling pumps. Each pump was connected to a 4-L polyethylene bag. A rechargeable battery was used to power the pumps and the timer. Air was delivered to the pumps through a common manifold connected to an external probe that extended to a height of 1 m above ground level. The pressure drops inside the system's individual lines and pump valves prevented cross-contamination among the samples. The sampler was designed to take sequential 1-h samples for a total of 6 h. This was accomplished by using a single-board computer programmed to control the relay board that switched power in sequence to pumps. All the equipments were housed in a polyethylene tote box.

The  $\text{SF}_6$  concentrations of integrated tracer samples were analyzed using a bank of four UCR constructed gas chromatographs, equipped with a

$\frac{1}{8}$ -in diameter Molecular Sieve  $5 \text{ \AA}$  column, electron capture detectors and a six-port gas sampling valve with a 2 mL sample loop. This analysis system could be loaded with 40 samples to determine their  $\text{SF}_6$  concentration simultaneously.

The tracer studies resulted in 40-h-long experimental periods. Out of these, 21 had sufficient concentration measurements to allow estimation of horizontal plume spread and centerline concentrations on each arc. This paper examines these 21 "experiments" in detail.

## 2.2. Meteorological measurements

Measurements of surface winds and winds aloft (up to  $\sim 600 \text{ m}$ ) were made using sonic anemometers and remote sensing acoustic sodars. A sonic anemometer, with its sensor placed at a height of 3 m, and a minisodar were collocated at an open area of the release site. The location of the instruments is shown in Fig. 1 as "Met. Site 1". A second sonic anemometer at a height of 3 m and a Model 2000 acoustic sodar were placed in an open area at Los Angeles County Sanitation District's Joint Water Pollution Control Plant (JWPCP), located  $\sim 4000 \text{ m}$  downwind of the source. A remote sensing microwave temperature sounder was used to determine the vertical temperature profile from the surface to 600 m above ground level at this downwind monitoring site. The location of the instruments is shown in Fig. 1 as "Met. Site 2".

The three components of velocity and temperature were sampled at 10 Hz using sonic anemometers. These measurements were used to derive 1-h averaged mean winds and temperatures, standard deviations of the turbulent velocity fluctuations, and turbulent momentum and heat fluxes. Winds and turbulence above the urban canopy was measured using the minisodar that took measurements from 15 m up to 200 m at a resolution of 5 m, and the full sized sodar which provided information up to heights of 600 m above ground level.

The meteorological measurements provided vertical profiles of wind speed, turbulence, and temperature, which were used to construct the meteorological inputs of the dispersion model described in this paper.

## 3. Behavior of meteorological variables

The Wilmington experiment yielded  $\sim 1$  month of mean wind and turbulence data covering a wide

variety of meteorological conditions. Fig. 2 compares the friction velocities and the kinematic heat fluxes measured at two meteorological sites during two of the study days. On 9/3/2004, the friction velocities and heat fluxes follow each other in time, while on 9/9/2004, the friction velocity at the downwind site does not start increasing until 11:00. We believe that this lack of correlation in time is related to the fact that the height of measurement at the downwind site is within the urban canopy, and is thus likely to be affected by channeling effects; in general, the friction velocities at the downwind site are smaller, which supports the hypothesis that the sonic is within the urban canopy (Rotach, 1993). The heat fluxes at the two sites are well correlated in time, with the heat flux in the downwind site being smaller than that at the release site.

The experiments were conducted during daytime hours when the whole area of the field study was dominated by south or southeast onshore flows. The surface boundary layer was convective for most of the experiments, except for the 24th trial conducted on 9/3/2004 at 7 a.m. Fig. 3 shows profiles of potential temperatures measured on 9/3/2004 at about 5000 m inland from the shore. The time evolution of these profiles is typical of those

observed during the 6 h of the day during which the field study was conducted. The boundary layer is still stable before 8 a.m. The convective boundary layer starts developing around 9 a.m. and reaches a height of 170 m at noon and does not grow any higher during the course of the day. The effects of this relatively shallow convective boundary layer on dispersion are discussed later.

Fig. 4 shows an example of the meteorological profiles for hour 8 on 27 August measured by the minisodar at the release site. In most cases, the data above 120 m were not considered valid because the signal-to-noise ratio of the sodar return was below unity at these heights. The co-ordinate system used here has its  $x$ -axis along the east–west direction, and  $y$ -axis along the north–south axis. The  $u$  component refers to the  $x$ -axis, and the  $v$  component to the  $y$ -axis. The mean velocity shown in the figure is the magnitude of the mean vector wind. The lateral turbulent velocity  $\sigma_v$  corresponds to a co-ordinate system in which the  $x$ -axis lies along the mean wind, and is obtained from the horizontal turbulent velocity fluctuations measured in the east–west and north–south co-ordinate system.

Fig. 4 indicates that the turbulence extends through 120 m even though the temperature profiles

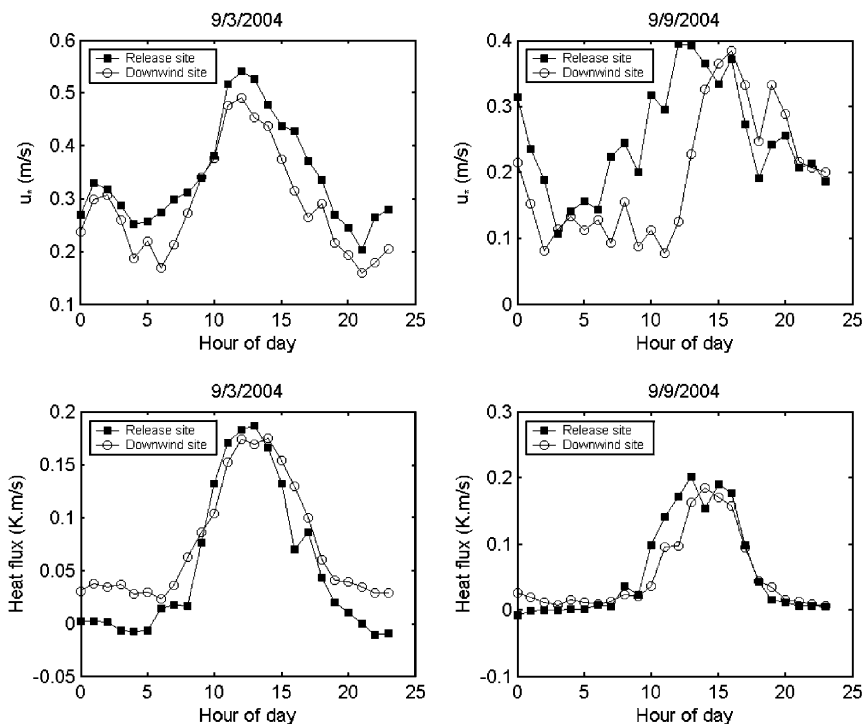


Fig. 2. Comparison of surface friction velocities and heat fluxes measured by sonic anemometers at LADWP (release site) and JWPCP (downwind site) on 9/3/2004 and 9/9/2004.

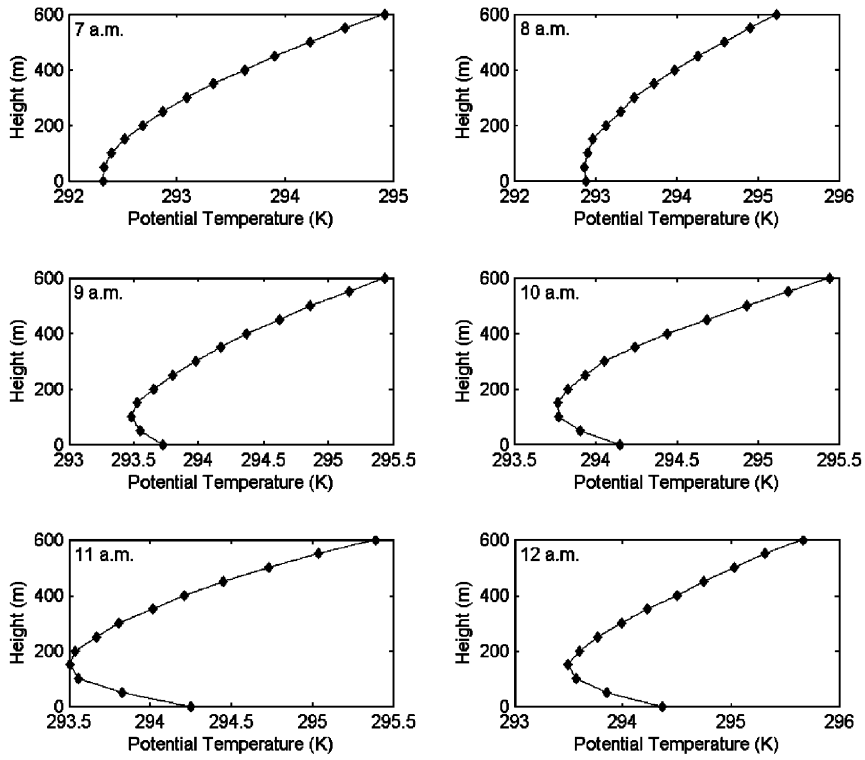


Fig. 3. Profiles of potential temperatures measured on 9/3/2004 at downwind site.

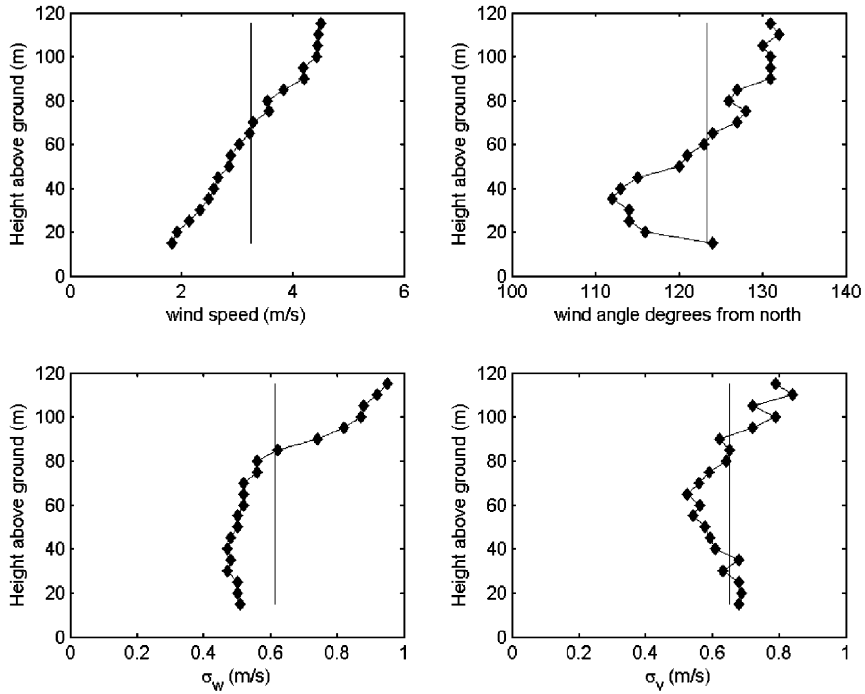


Fig. 4. Meteorological profiles observed on hour 8 on 8/27/2004 at release site. Vertical lines represent medians of the variables.

of Fig. 3 indicate that boundary layer is stable above 100 m at 8 a.m.; the rapid increase in  $\sigma_w$  above 80 m might be related to noise in the sodar data. Thus, turbulent mixing can extend well beyond the height at which the potential temperature gradient becomes positive. We believe that when the convectively generated boundary layer is shallow, the vertical extent of turbulent mixing is determined by the height of a shear generated boundary layer that is advected with the onshore flow. We support this hypothesis through analysis of measured ground-level concentrations.

The height range of valid data from the sodar was 15 m to about 100 m. We took the measured values at 50 m to be representative of the boundary layer relevant to dispersion. These values were used as inputs to the dispersion model, which is described next. Fig. 5 shows that the standard deviation of the vertical velocity fluctuations is correlated with the mean wind, which supports our contention that the measured turbulence is generated by shear during most of the experimental hours.

Fig. 6 shows the range of meteorological variables sampled in the field experiment. The turbulent intensities vary from 0.17 to as large as 1.1 during an experiment in which the wind speed dropped below  $1 \text{ m s}^{-1}$ . The mean horizontal intensity is 0.21

while the mean vertical intensity is 0.19. The transport winds used in the model vary from  $<1$  to  $5 \text{ m s}^{-1}$ .

#### 4. Dispersion parameters

We estimated the horizontal plume spreads by assuming that the maximum concentration measured on each arc corresponded to the plume centerline. We assumed that  $\sigma_y$  did not vary along the arc so that the concentrations were described by

$$C(x, y) = C_{\max} \exp\left(-\frac{y^2}{2\sigma_y^2}\right). \quad (1)$$

Then,  $\sigma_y$  was obtained by fitting the following equation to the data from each arc:

$$\ln\left(\frac{C_{\max}}{C}\right) = \frac{1}{2\sigma_y^2} y^2. \quad (2)$$

The slope of the fitted line was used to compute  $\sigma_y$ . We adjusted the  $\sigma_y$  determined from Eq. (2) until we obtained the best fit between estimated and observed concentrations along each arc. Fig. 7 illustrates examples of estimated concentration profiles compared with observed concentrations on hour 11, 9/2/2004.

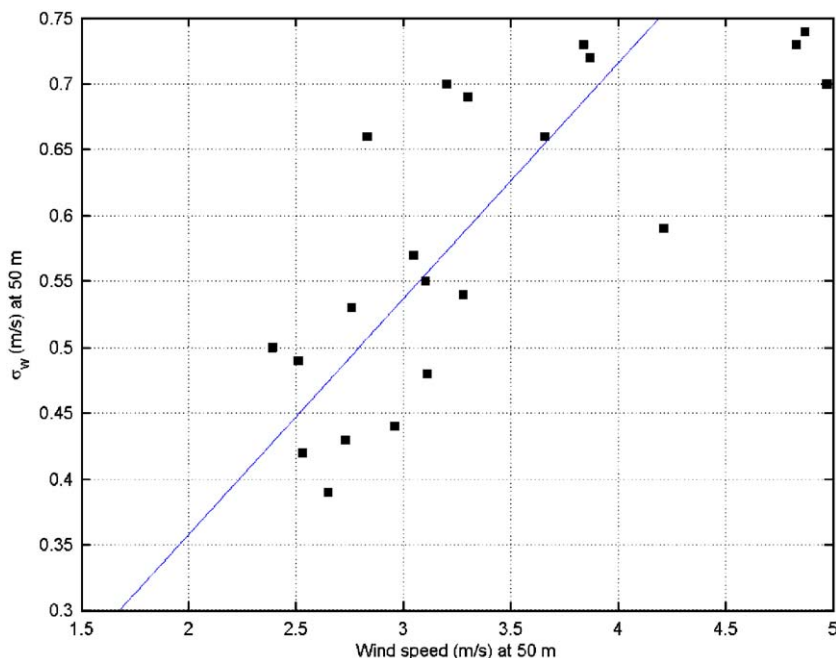


Fig. 5. Relationship between  $\sigma_w$  and mean wind speed measured at 50 m. The slope of the line is about 0.2.

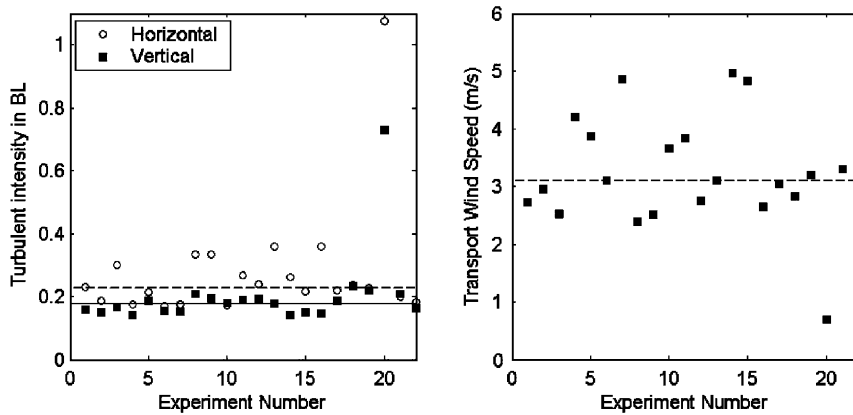


Fig. 6. Variation of turbulent intensities and transport wind speeds used in the dispersion model. Horizontal lines correspond to mean values of the variables.

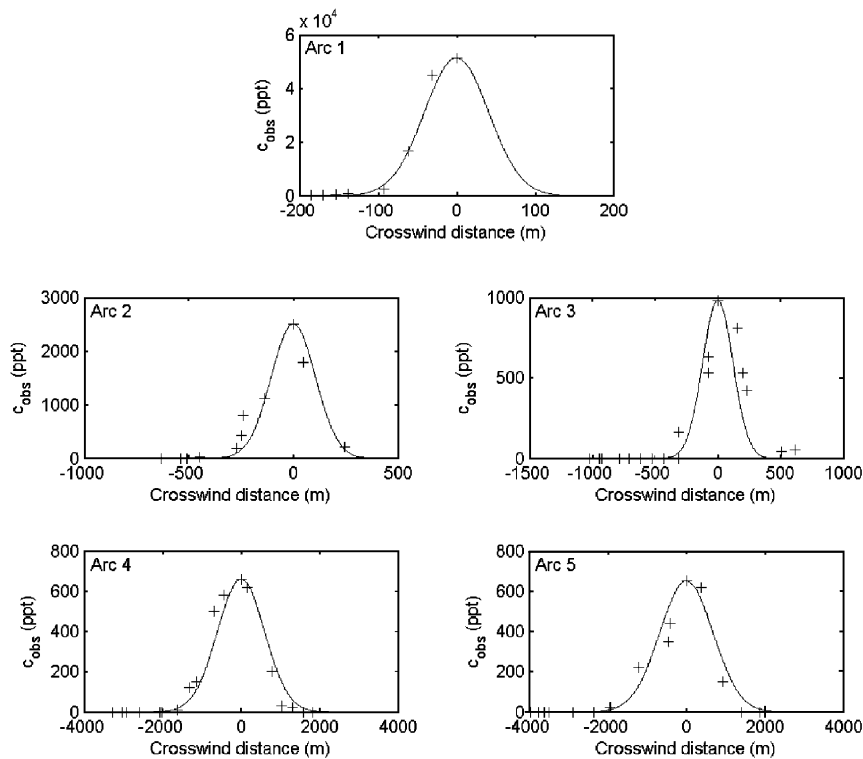


Fig. 7. Crosswind concentration profiles measured on 9/2/2004 at 11:00.

The vertical plume spreads were inferred from a Gaussian dispersion model using the maximum ground-level concentrations and the mean wind discussed earlier:

$$\sigma_z = \frac{Q}{\pi U \sigma_y C_{\max}}, \quad (3)$$

where  $Q$  is the source strength and  $U$  the transport wind speed.

Fig. 8 shows the variations of the observed horizontal and vertical plume spreads with downwind distances averaged over all the runs for two sets of experiments: one corresponding to releases inside the cluster of buildings in the LADWP power

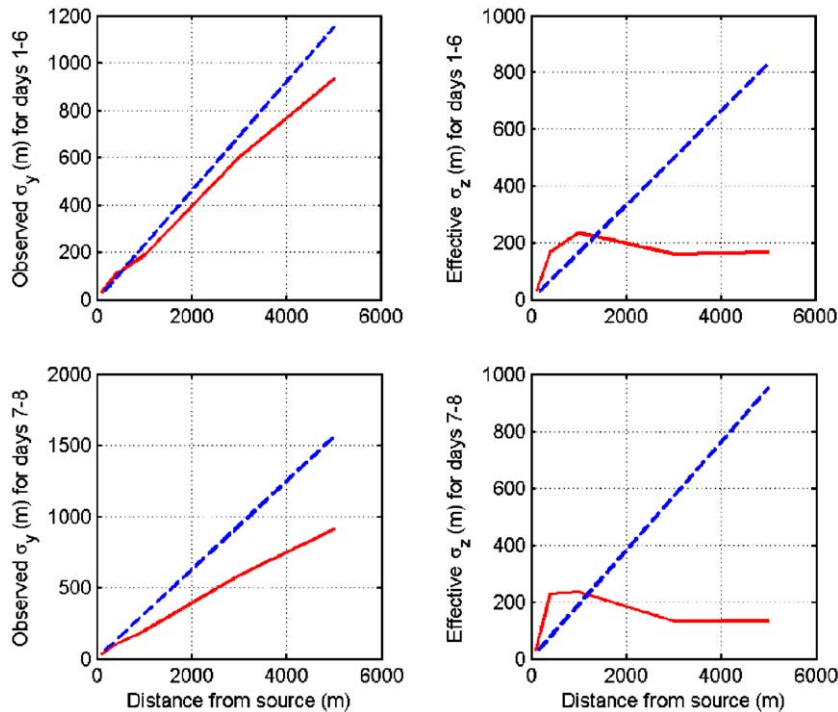


Fig. 8. The variation of dispersion parameters as a function of downwind distance. The dashed straight lines represent linear growth determined by turbulent intensities.

plant, and the other to releases in an open area close to the power plant. This division was designed to examine the importance of building enhanced plume spread. The first set of releases was conducted during the first 6 days of the experiment, and the second set during the last 2 days.

The dashed straight lines in the figures correspond to the equations  $\sigma_z = i_z x$  and  $\sigma_y = i_y x$ , where  $i_z = \sigma_w/U$  and  $i_y = \sigma_v/U$  are the vertical and horizontal turbulent intensities. The growth rate of the observed horizontal spread is less than linear and can be represented by

$$\sigma_y = \frac{i_y x}{(1 + x/L_y)^{1/2}}, \quad (4)$$

where  $i_y$  is the horizontal turbulent intensity at a height of 50 m. The length scale,  $L_y$ , was taken to be 2500 m, a value suggested by Briggs (1973) for use in urban areas on the basis of his analysis of the St. Louis experiment (McElroy and Pooler, 1968).

Fig. 9 indicates that estimates of  $\sigma_y$  from Eq. (4) compare well with observed values for the first 6 days (Fig. 9a) as well as the last 2 days (Fig. 9b) of experiments. It appears that there is no need to invoke initial building induced horizontal plume

spread to explain the observations made during the first 6 days of the experiment when the releases occurred within the power plant building structure.

We see from Fig. 8 that  $\sigma_z$  first grows rapidly and then levels off around 1000 m from the release. The decrease in  $\sigma_z$  with distance seen in the figures is caused by the uncertainties in observations introduced in Eq. (3). It appears from Fig. 8 that the growth of  $\sigma_z$  is limited by the height of a shear generated boundary layer, which is discussed in detail in Section 5.

## 5. Concentration data analysis

Fig. 10 shows the variation of the arc maximum concentrations with distance from release; each point is obtained by averaging over maximum concentrations observed at each arc. The straight lines correspond to  $C_{\max} \sim 1/x^2$ , which is the variation that would result if the plume spreads grew linearly with distance. We see that the concentrations decrease at a slower rate than  $x^{-2}$  after a distance of about 1000 m from the source. There is little difference in the variation of concentrations for the two sets of releases except

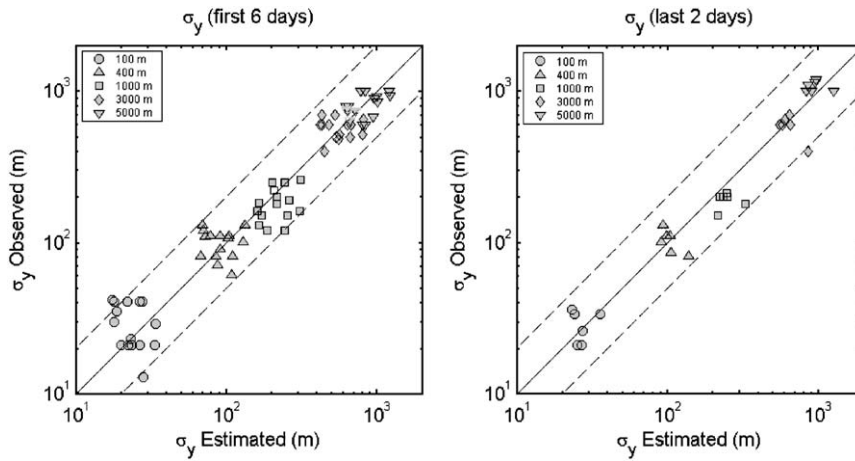


Fig. 9. Comparison of measured horizontal plume spreads with model estimates during the (a) first 6 days and (b) last 2 days of experiments.

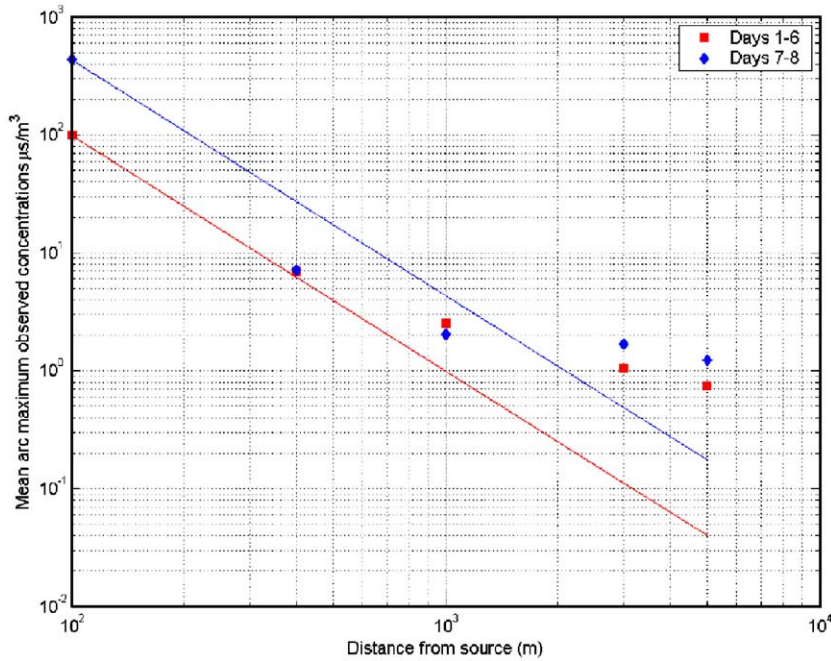


Fig. 10. The variation of observed arc maximum concentrations with downwind distance.

close to the source. The maximum concentrations on the 100 m arc are about four times lower for the release in the power plant complex compared to those in the open area next to the plant. This is related to the initial plume spread induced by the power plant buildings.

These measured maximum concentrations were analyzed using a simple dispersion model that assumes Gaussian distributions in the horizontal

and vertical directions. The concentration is given by

$$\frac{C(x, y = 0, z = 0)}{Q} = \frac{1}{\pi U \sigma_y \sigma_z} \exp\left(-\frac{h_s^2}{2\sigma_z^2}\right), \quad (5)$$

where  $x$  is the downwind distance from release,  $h_s$  the release height, and  $U$  the transport wind speed. The horizontal plume spread is given by Eq. (4).

The vertical spread is taken to be

$$\sigma_z = \frac{\sigma_w x}{U}. \quad (6)$$

Model performance is described in terms of the statistics of the ratio  $C_p/C_o$ , where  $C_o$  and  $C_p$  refer to the observed and predicted concentrations, respectively. Then, the bias in the model estimate is characterized by  $m_g$ , the geometric mean of the ratio:

$$m_g = \exp(\text{mean}(\varepsilon)),$$

where

$$\varepsilon = \log\left(\frac{C_p}{C_o}\right), \quad (7)$$

and the spread of observations about a model estimate is quantified using the geometric standard deviation,  $s_g$ ,

$$s_g = \exp(\text{standard deviation of } \varepsilon). \quad (8)$$

Then, if the observed concentrations are lognormally distributed about the model estimate, the 95% confidence interval of the ratio of the observed to the estimated concentration is approximately given by the interval  $m_g s_g^{1.96}$  to  $m_g s_g^{-1.96}$ .

We first examined the concentrations collected on the first 6 days of the experiments when the release occurred behind the power plant. The left panel of Fig. 11 compares observed ground-level concentration maxima, normalized by the emission rate, with estimates using Eqs. (4) and (6) for plume spread. Because the plots compare the estimated maximum on each arc with the observed maximum on the same arc, the points in the plot do not always correspond to the same receptor. The model over-

estimates the concentrations in the first two arcs but underestimates the ground-level concentrations on the 3000 and 5000 m arcs.

The right panel of Fig. 11 shows the effects of making two modifications to the model. The first involves using an initial vertical plume spread,  $\sigma_{z_0}$ , induced by the power plant building behind which the releases occurred. If we assume that the plume is well mixed through the building height of 40 m,  $\sigma_{z_0}$  works out to be 32 m which is  $\sqrt{2/\pi} = 0.8$  times the height of the building. Incorporating initial plume spread eliminates the overestimation on the 100 and 400 m arcs.

The second modification is associated with limiting vertical dispersion to the height of a boundary layer, which is discussed in more detail in next paragraphs. This reduces the underestimation of concentrations on the 3000 and 5000 m arcs, as seen in the right panel of Fig. 11.

The boundary layer was initially taken to be that of the TIBL given by (Venkatram, 1977)

$$h_T = \left(\frac{2Q_0 x}{\gamma U}\right)^{1/2}, \quad (9)$$

where  $Q_0$  is the surface kinematic heat flux,  $\gamma$  the overwater potential temperature gradient, and  $U$  the transport wind speed. We averaged the measured kinematic heat fluxes at the two sites to estimate  $Q_0$  required in Eq. (9). The  $\gamma$  was obtained from the temperature profile measurements at the downwind site, and was taken to be the potential temperature gradient above the convective boundary layer. It turned out that Eq. (9) generally predicted TIBL heights that were about twice the

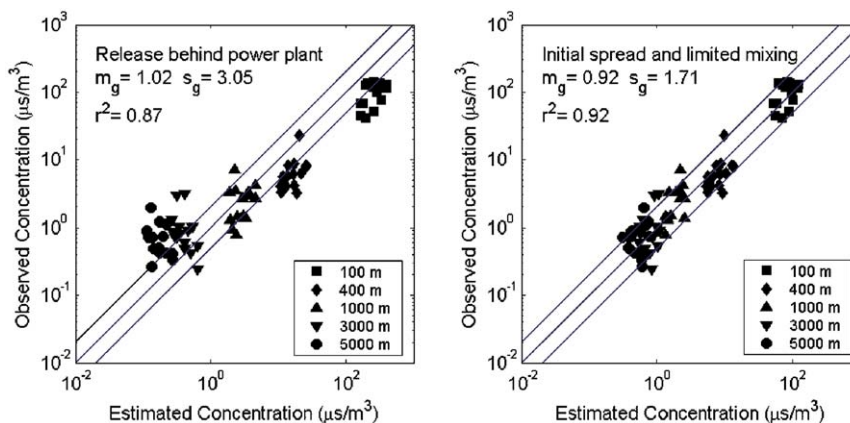


Fig. 11. Comparison of measured arc maximum concentrations with model estimates during the first 6 days of the experiment. Right panel corresponds to modifications described in the text.

observed heights, which did not exceed 200 m. Its use in the model did not yield improvements in model performance.

The improvement seen in the right panel of Fig. 11 was obtained by limiting the vertical mixing to the height of a shear generated boundary layer given by

$$h_{sh} = 8 \frac{\sigma_w}{N}, \tag{10}$$

where  $N$  is the Brunt–Vaisala frequency given by

$$N = \left( \frac{g}{T_o} \gamma \right)^{1/2}. \tag{11}$$

The factor 8 is an empirical constant whose value is consistent with that suggested by Laikhtman (1961) if we take  $\sigma_w/U \approx 0.2$ .

Using  $\sigma_w$  as a surrogate for the surface friction velocity that created the boundary layer is

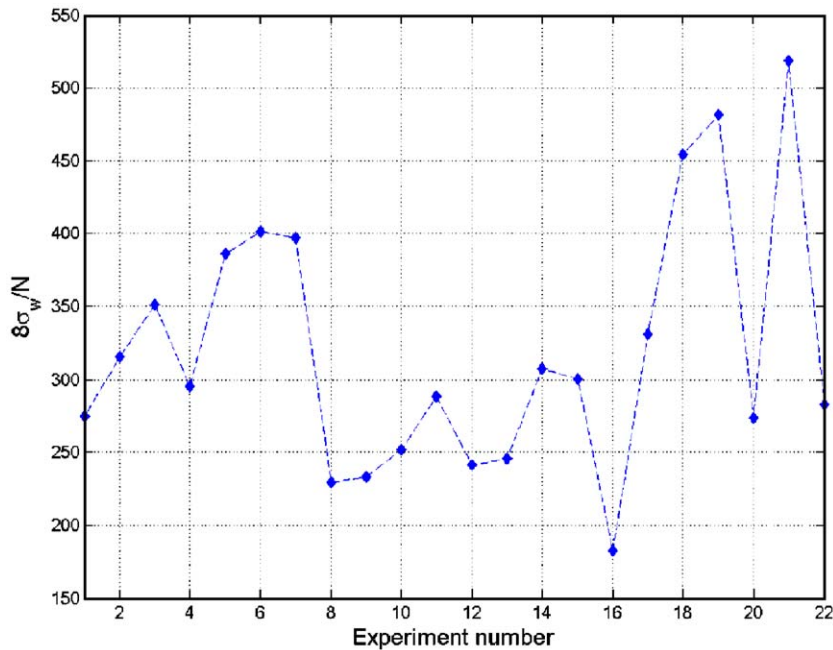


Fig. 12. Variation of the shear generated boundary height during the field study.

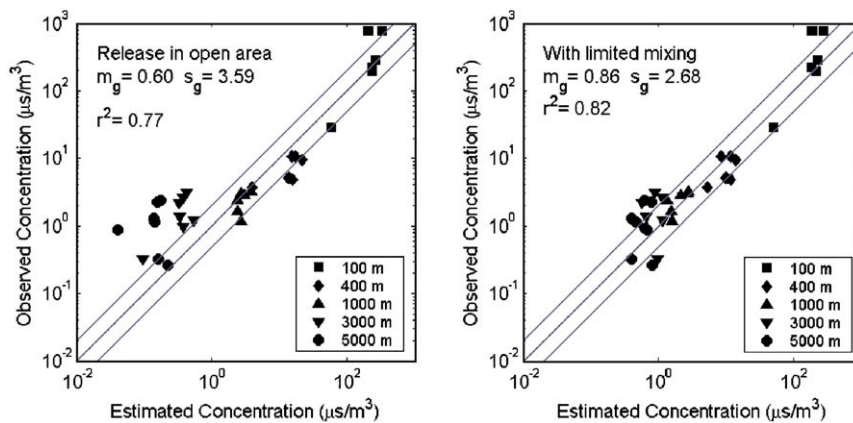


Fig. 13. Comparison of measured arc maximum concentrations with model estimates during the last 2 days of the experiment. Right panel corresponds to modifications described in the text.

supported by the correlation between  $\sigma_w$  and  $U$  seen in Fig. 6. Fig. 12 shows that  $h_{sh}$  varies over a wide range, from 170 m to over 500 m, suggesting that it does not serve as an empirical fitting parameter.

Then, vertical spread plume is modified to

$$\sigma_z = \min\left(\frac{\sigma_w x}{U} \left(1 + \frac{x}{L_z}\right)^{1/2}, \sqrt{\frac{2}{\pi}} h_{sh}\right), \quad (12)$$

where the length scale,  $L_z$ , is taken to be the height of the boundary layer,  $h_{sh}$ . The  $x^{3/2}$  growth incorporated in Eq. (12) models the faster than linear growth observed in Fig. 8, and is consistent with behavior of vertical spread of surface releases in the convective boundary layer (Nieuwstadt, 1980, for example).

There is only indirect evidence of the shear generated boundary layer determining the vertical extent of mixing. Postulating its presence results in major improvements in model performance: the error standard deviation decreases dramatically from 3.05 to 1.71, although  $m_g$  is about the same value.

Fig. 13 shows the improvement in model performance when Eq. (12) was used to estimate vertical spread for the last 2 days of the experiment. Because the release was in open ground, the vertical spread was not corrected for initial spread. We see that the bias improves from 0.60 to 0.86 and the error standard deviation decreases from 3.59 to 2.68.

## 6. Conclusions

The analysis of the meteorological and the dispersion data collected during the Wilmington experiment indicate that:

1. Even during summer, the stability of the onshore flow can be strong enough to keep the height of thermal internal boundary layer below 150 m at distances of 5000 m from the shoreline. However, turbulence levels in the capping stable layer are comparable to those measured close to the surface. We suggest that this turbulence is associated with a shear generated boundary layer that is advected with the onshore flow.
2. Vertical dispersion of a ground-level release is limited to the height of this shear generated boundary layer. The height of this boundary layer can be estimated as  $8\sigma_w/N$ . This conclusion is tentative because its presence is inferred only through the improvement in model performance.
3. The data indicate that it is necessary to account for building induced vertical spread when the release is close to a building. This conclusion confirms results from other similar studies (Hanna et al., 2003).

## Acknowledgements

The research summarized in this paper was funded by the California Energy Commission and California Air Resources Board.

We thank the anonymous reviewers for their valuable comments, which resulted in major improvements to the paper.

*Disclaimer:* The research presented here was performed under the Memorandum of Understanding between the US Environmental Protection Agency (EPA) and the US Department of Commerce's National Oceanic and Atmospheric Administration (NOAA) and under agreement number DW13921548. This work constitutes a contribution to the NOAA Air Quality Program. Although it has been reviewed by EPA and NOAA and approved for publication, it does not necessarily reflect their policies or views.

## References

- Briggs, G.A., 1973. Diffusion estimation for small emissions. ERL, ARL USAEC Report ATDL-106. US Atomic Energy Commission, Oak Ridge, TN.
- Hanna, S., Britter, R., Franzese, P., 2003. A baseline dispersion model evaluated with Salt Lake City and Los Angeles tracer data. *Atmospheric Environment* 37, 5069–5082.
- Laikhtman, D.L., 1961. Physics of the boundary layer of the atmosphere. Translated by the Israel Program for Scientific Translations, Jerusalem, 1964. Available from the Office of Technical Services, US Department of Commerce, Washington, DC, 200pp.
- Luhar, A.K., Sawford, L.B., 1996. An examination of existing shoreline fumigation models and formulation of an improved model. *Atmospheric Environment* 30, 609–620.
- McElroy, J.L., Pooler, F., 1968. The St. Louis Dispersion Study—Analysis, vol. II. National Air Pollution Control Administration, Publication No. AP-53. US DHEW Arlington, 50pp.
- Misra, P.K., Onlock, S., 1982. Modelling continuous fumigation of Nanticoke generating station plume. *Atmospheric Environment* 16, 479–489.
- Nieuwstadt, F.T.M., 1980. Application of mixed layer similarity to the observed dispersion from a ground-level source. *Journal of Applied Meteorology* 19, 157–162.
- Rotach, M.W., 1993. Turbulence close to a rough urban surface. Part I: Reynolds stress. *Boundary-Layer Meteorology* 65, 1–28.
- Venkatram, A., 1977. A model of internal boundary-layer development. *Boundary-Layer Meteorology* 11, 419–437.